

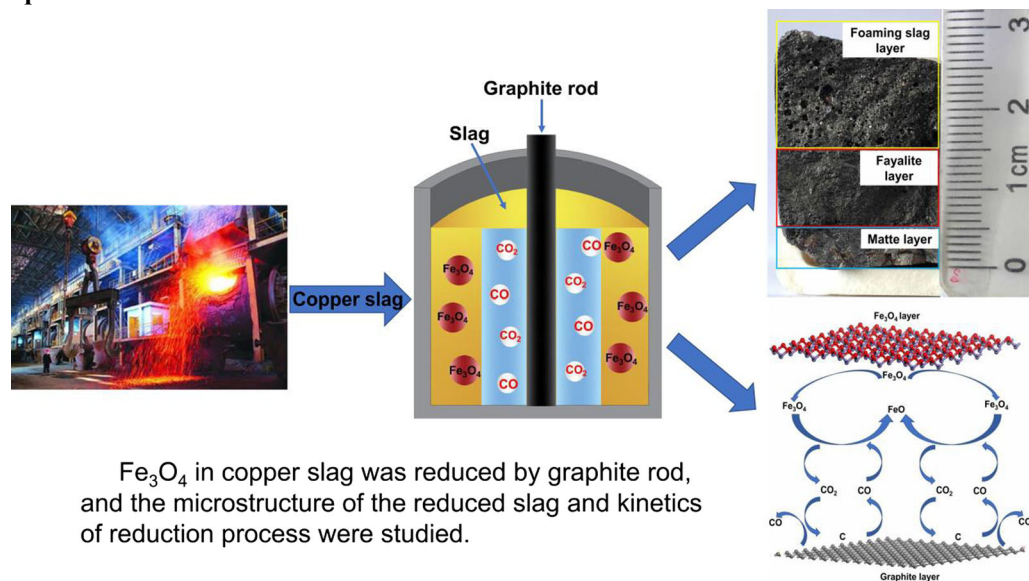
Reduction of Magnetite from Copper Smelting Slag in the Presence of a Graphite Rod



HAIPEI ZHANG, BO LI, YONGGANG WEI, HUA WANG, YINDONG YANG, and ALEXANDER MCLEAN

Through the reduction reaction of Fe_3O_4 and graphite rod, the viscosity of slag was reduced and the settlement of matte in slag was promoted. The reduction of Fe_3O_4 in copper slag by a graphite rod was studied and the kinetics of the reduction process analyzed. The results show that the content of Fe_3O_4 decreased with increase in reduction temperature and reduction time. The slag samples after reduction were examined and found to consist of three layers: a slag foam layer, a fayalite layer, and a matte layer. A substantial number of large-sized matte particles were found in the slag foam layer. Also, a layer of Fe_3O_4 was attached to the upper surface of the matte layer. The reduction of Fe_3O_4 was concluded to be a second-order reaction, the apparent activation energy was 610 kJ/mol, and the limiting step was the Boudouard reaction.

Graphical Abstract



Fe_3O_4 in copper slag was reduced by graphite rod, and the microstructure of the reduced slag and kinetics of reduction process were studied.

<https://doi.org/10.1007/s11663-020-01963-0>

© The Minerals, Metals & Materials Society and ASM International 2020

HAIPEI ZHANG and HUA WANG are with the State Key Laboratory of Complex Nonferrous Metal Resources Clean Utilization, Kunming University of Science and Technology, Kunming 650093, Yunnan Province, China and also with the Faculty of Metallurgy and Energy Engineering, Kunming University of Science and Technology, Kunming 650093, Yunnan Province, China. BO LI and YONGGANG WEI are with the State Key Laboratory of Complex Nonferrous Metal Resources Clean Utilization, Kunming University of Science and Technology and also with the Faculty of Metallurgy and Energy Engineering, Kunming University of Science and Technology and also with the Department of Materials Science and Engineering, University of Toronto, Toronto M5S3E4, Canada. Contact e-mail: libokmust@163.com YINDONG YANG and ALEXANDER MCLEAN are with the Department of Materials Science and Engineering, University of Toronto.

Manuscript submitted May 3, 2020.

Article published online October 7, 2020.

I. INTRODUCTION

IN the smelting process of copper, oxygen-enriched air bath smelting is widely used because of its high production capacity, low fuel consumption, and high adaptability for raw materials. However, high oxygen potential will lead to the enrichment of Fe_3O_4 in the slag^[1,2] which then needs to be diluted by a combination of direct-current dilution and reductant dilution in the electric furnace.^[3] Dilution can promote the aggregation and growth of copper droplets, and enhance separation of slag and copper. Reduction of Fe_3O_4 decreases the slag viscosity and promotes the settling of copper particles.^[4,5]

There are two main forms of copper loss in slag: physicochemical losses and mechanical entrained losses. Slag viscosity is one of the important factors affecting the mechanical entrainment loss of copper.^[6] Therefore, it is particularly important to reduce the viscosity and melting point of the slag by reducing Fe_3O_4 to FeO , which then combines with SiO_2 to form fayalite.

Reddy *et al.*^[7] studied the reduction of Cu_2O from artificial slag by carbon. The reduction was a first-order reaction and the limiting step was chemical reaction at the slag/graphite interface. Argon stirring had no effect on the kinetics of the reduction reaction. Sharif^[8] studied the reduction of PbO in $\text{PbO-CaO-SiO}_2\text{-FeO}_x\text{-MgO}$ slags by CO-CO_2 gas mixture. The deduced apparent first-order rate constant increased with increasing iron oxide content, oxidation state of the slag, and temperature. The limiting step was the rate of formation of CO_2 at the gas-slag interface. Li^[9] studied the reduction of Fe_3O_4 in copper slag using waste cooking oil. The results showed that the content of Fe_3O_4 in the slag decreased with the increase in reduction time. Increasing temperature was also beneficial to the reduction of Fe_3O_4 . In the reduction process, Fe_3O_4 gradually transforms to fayalite, and the viscosity of the slag decreases. Zhou *et al.*^[10] studied the reduction of oxides in copper slag by anthracite. Again, reducing the content of Fe_3O_4 was beneficial for reducing the viscosity of slag. Copper droplets coalesce and grow in the process of settling, and some are encapsulated by Fe_3O_4 particles to form composite $\text{Cu-Fe}_3\text{O}_4$ droplets.

In this paper, graphite is used as a reducing agent to reduce Fe_3O_4 in slag and reduce the viscosity of slag. It solves the problem that matte can not settle smoothly due to the high viscosity of copper slag, resulting in the high content of copper in slag. It provides a new way to recover matte from copper slag. X-ray diffraction (XRD) and electron probe microanalysis (EPMA) were used to analyze the slag samples, the phase composition, and the microstructure of the different layers of the slag. The reduction kinetics of Fe_3O_4 was also studied and the apparent activation energy determined. The results provide a theoretical basis for the dilution process of copper slag using a carbonaceous reducing agent.

II. EXPERIMENTAL ASPECTS

A. Materials

The copper smelting slag used for the experiments was provided by Yunnan Copper Inc. The chemical analysis is shown in Table I from which it can be seen that the contents of Cu, Fe (Total), SiO_2 , and S in the slag are relatively high: 17.82 pct, 33.06 pct, 19.13 pct, and 8.07 pct, respectively. The content of Fe_3O_4 is 12.9 pct.

As indicated in Figure 1, the results of XRD analysis indicate that the main phases present in the slag are fayalite, magnetite, and matte.

B. Experimental Method and Analytical Techniques

In order to keep the contact area between reductant and molten slag stable, a graphite rod was used as the reductant. 300 g slag powder contained in a corundum crucible (63 mm inside diameter) was placed in the constant temperature zone of a tubular furnace. After exhausting the air from the furnace using a vacuum pump, nitrogen at a flow rate of 600 mL/min provided a protective atmosphere. The slag sample was heated to the experimental temperature (1250 °C, 1275 °C, 1300 °C, 1325 °C) at a heating rate of 10 °C/min and held at constant temperature for 30 min. Subsequently, the graphite rod (diameter: 12 mm) was inserted into the molten slag. The reduction times were 0, 15, 30, 45, 60, 75, and 90 minutes. After reduction, the graphite rod and the slag were separated, and the slag was cooled to room temperature and analyzed.

The content of Fe_3O_4 in the slag was determined by magnetic susceptibility method with a SATMAGAN 135 instrument. The accuracy was 0.4 pct. The phase composition of the copper slag was determined using a Japan Science D/max-R diffractometer. The diffraction spectra in the range 10° to 90° at a rate of 10°/min were measured. The morphological structure and composition of the slag were determined using a JEM-2100 electron probe microanalyzer.

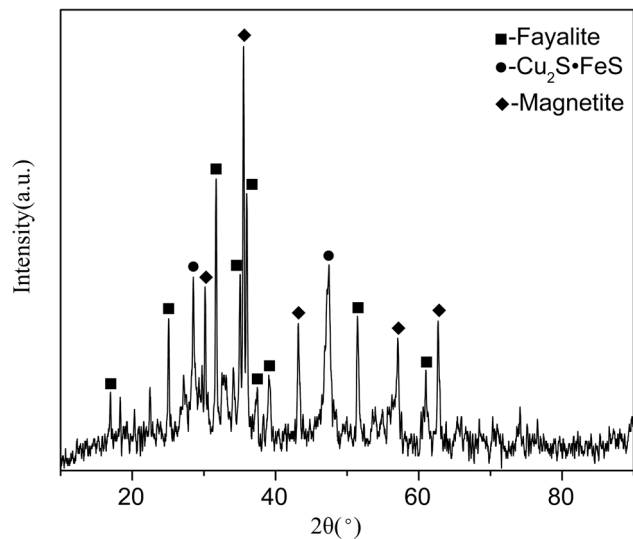


Fig. 1—XRD pattern of copper smelting slag.

Table I. Chemical Composition of the Slag Sample

Component	Cu	Fe (Total)	SiO_2	S	Al_2O_3	CaO	MgO	ZnO	Fe_3O_4
Content Weight Percent	17.82	33.06	19.13	8.07	2.96	2.12	1.95	1.83	12.9

III. RESULTS AND DISCUSSION

A. Effect of Reduction Time and Temperature on Fe_3O_4 Content in Slag

Figure 2 shows the relationship between Fe_3O_4 content in slag and reduction time at different temperatures. It can be seen that the Fe_3O_4 content as well as the reduction rate decreased with the increase in reduction time. The Fe_3O_4 content in slag decreases with the increase in reduction temperature at the same reduction time. When the temperature is higher, the reduction of Fe_3O_4 is increased. The slope of the line at the initial stage of the reaction at different temperatures increased with temperature, indicating that the reduction rate of

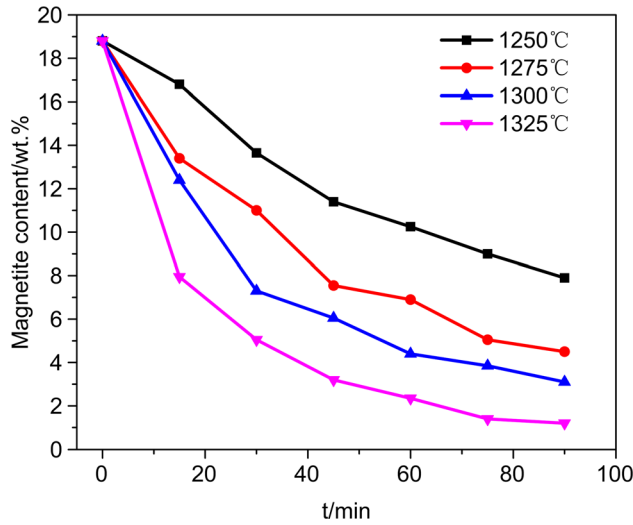


Fig. 2— Fe_3O_4 content in slag as a function of time at different temperatures.

Fe_3O_4 increased. The reason is that at higher temperatures slag fluidity is improved and hence mass transfer and diffusion of Fe_3O_4 in the slag are enhanced.

Figure 3 is the phase diagram of $FeO-Fe_3O_4-SiO_2$ ternary system at 1250 °C drawn by Factsage 7.2. Point a is the unreduced slag, and points b, c, d, and e are the positions of slag composition in the phase diagram when the reduction time is 15, 30, 60, and 90 minutes, respectively. According to the composition of unreduced slag, the composition of unreduced slag is located in the slag-liquid phase and spinel phase region. The existence of spinel phase with a high melting point is not conducive to the separation of slag and matte. With the increase of reduction time, the content of Fe_3O_4 in slag decreases, the composition point of slag gradually approaches the slag-liquid phase region, and the content

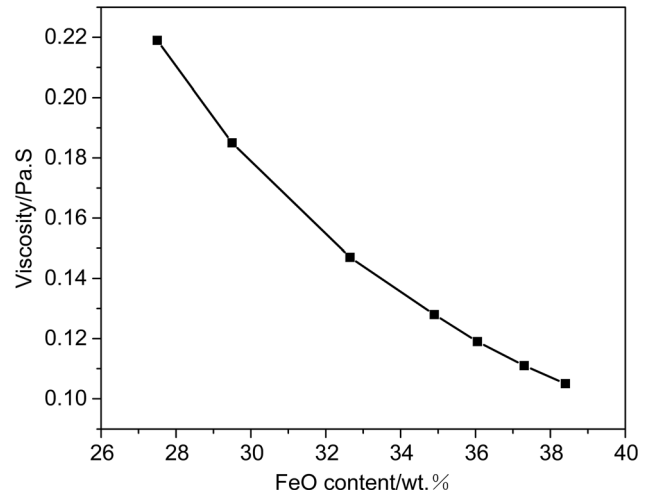


Fig. 4—Effect of FeO content on the viscosity of slag at 1250 °C.

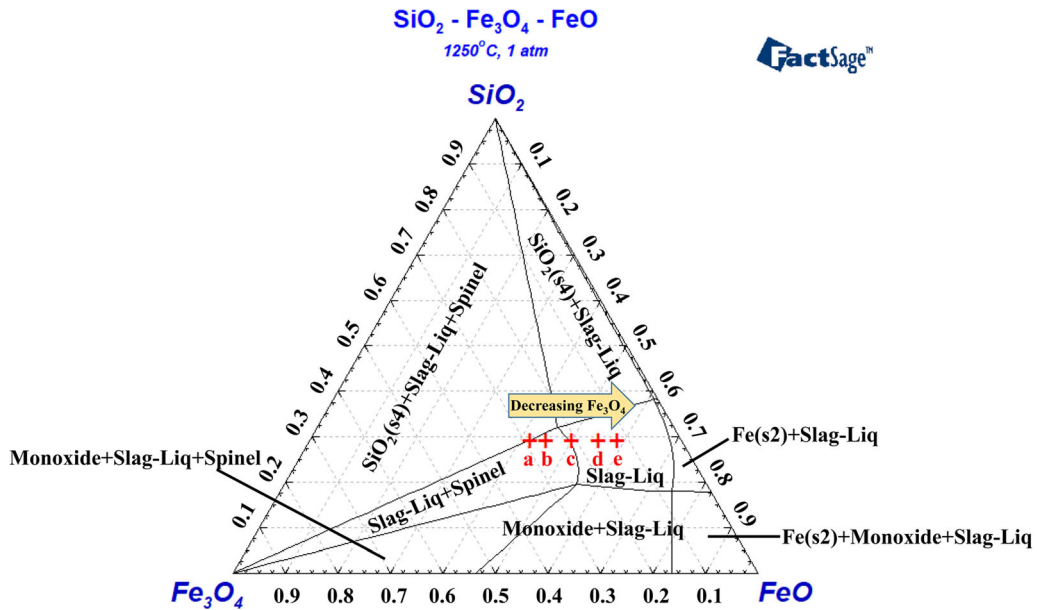


Fig. 3—Phase diagram of the $FeO-Fe_3O_4-SiO_2$ ternary system at 1250 °C.

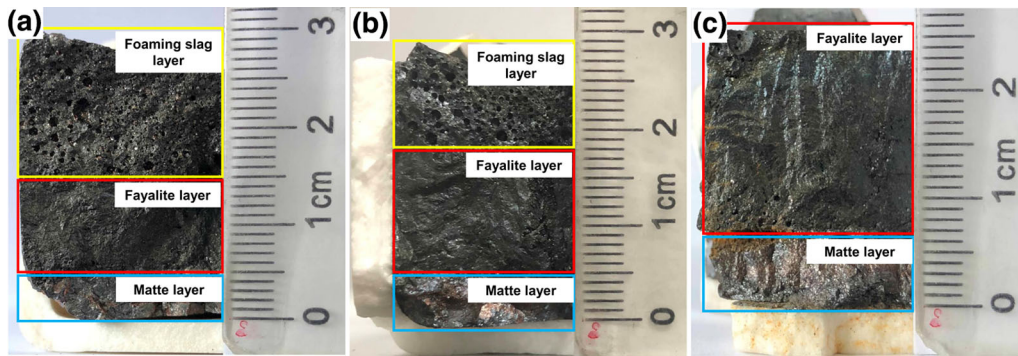


Fig. 5—Cross-sections of slag samples with reduction time of 30, 60, and 90 min, respectively, at 1250 °C: (a) 30 minutes; (b) 60 min; (c) 90 min.

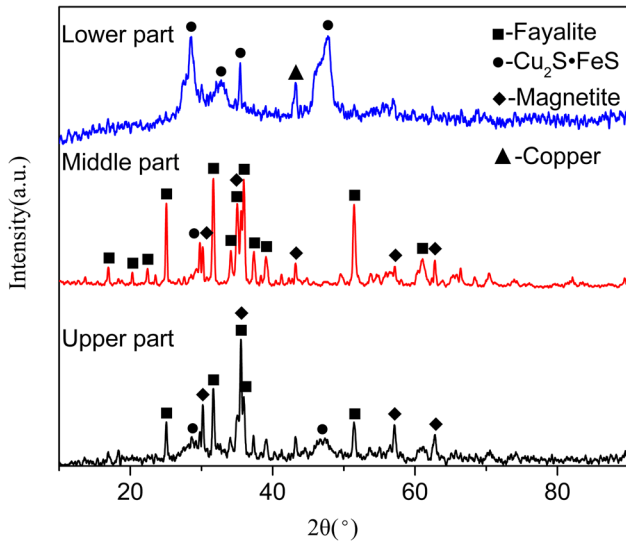


Fig. 6—XRD patterns of the upper, middle, and lower parts of slag with reduction time of 30 min at 1250 °C.

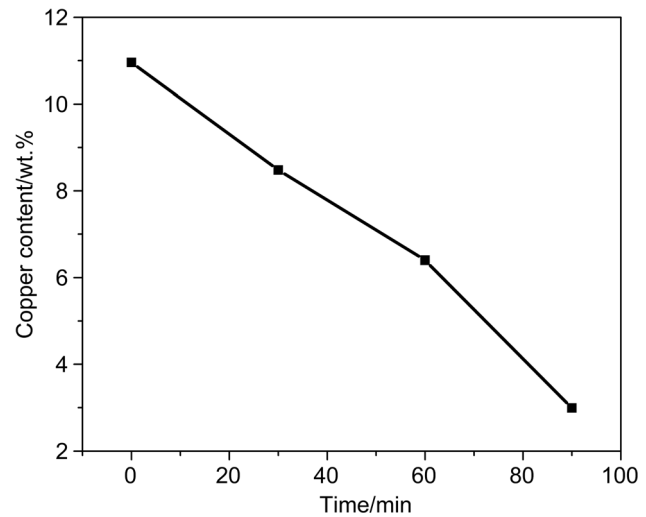


Fig. 7—Copper content of slag samples with different reduction time at 1250 °C.

of slag-liquid phase increases, which is conducive to the separation of matte and slag. Figure 4 shows the relationship between the FeO content in slag under different reduction time and the viscosity of slag at 1250 °C. It can be seen from the figure that the viscosity of slag decreases with the increase of FeO content in slag, which is conducive to the separation of slag and matte. The reason is that Fe_3O_4 in slag is continuously reduced to FeO with the increase of reduction time, FeO combines with SiO_2 in slag to form fayalite, which can reduce the viscosity and melting point of the slag.

Figure 5 shows the cross-sections of slag samples with reduction time of 30, 60, and 90 minutes at 1250 °C. As can be seen from Figure 5(a), the structure of the upper part of the slag contains many holes, mixed with metallic particles, confirming the formation of slag foam. The middle part of the slag is compact without holes. The color of the lower part is different from the other parts and shows a metallic luster. Phase analysis of the different parts was carried out by XRD and the results are shown in Figure 6, from which it can be seen that the main phases in the upper part are fayalite, magnetite and matte. The main phase in the middle part

is fayalite with a small amount of magnetite and matte while the main phase in the lower part is matte with a small amount of copper. According to this analysis, the reduced slag can be divided into three zones: the upper part is the slag foaming layer; the middle part is the fayalite layer; and the lower part is the matte layer. It can be seen from Figure 5 that the height of the foaming slag layer gradually decreases with the increase of reduction time, and when the reduction time is 90 minutes, the foaming slag has essentially disappeared. The main reason for the formation of foaming slag is as follows^[11,12]: when the viscosity of slag is high, the velocity of rising bubbles slows down, the stability of single bubbles becomes greater, and a larger amount of gas is retained in the slag, which results in a honeycomb structure. With the increase in reduction time, more Fe_3O_4 is reduced to FeO, fayalite is formed, which will reduce the slag viscosity, the gas bubbles rapidly rise to the surface of the slag and escape, thus nullifying the slag foaming behavior. Figure 7 shows the copper content of slag samples with reduction time of 30, 60, and 90 minutes at 1250 °C. It can be seen from the Figure 7 that the copper content in slag decreases with

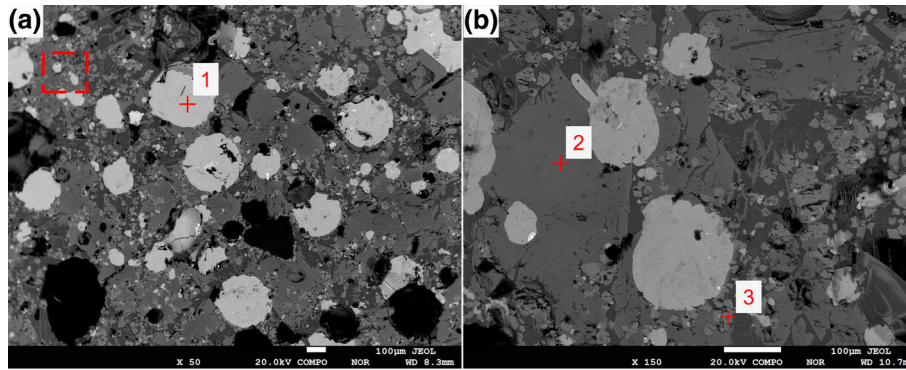


Fig. 8—Microstructure of the foaming slag layer with reduction time of 30 min at 1250 °C: (a) foaming slag layer; (b) enlarged view of (a).

Table II. Elemental Analysis of Different Points (Wt Pct)

Point	O	Si	S	Fe	Cu
1	0	0	25.46	11.19	65.35
2	30.83	15.01	0	48.02	0
3	23.78	0	0	76.22	0

the increase of reduction time. With the increase of reduction time, the content of Fe_3O_4 and viscosity of slag decrease, and this is beneficial for the settlement of matte droplets.

Figure 8(a) shows the microstructure of the foaming slag layer. Figure 8(b) is an enlarged view of the red marked area in Figure 8(a). Table II shows that the elemental compositions of point 1, point 2, and point 3 in Figure 8 correspond to the matte phase, fayalite phase, and magnetite phase, respectively. It can be seen from Figure 8(a) that there is a significant number of large-sized matte particles in the foaming slag layer. Figure 8(b) shows that matte particles are embedded in the fayalite phase, and many magnetite particles are adsorbed around the matte particles.

Figure 9 shows the microstructure of the fayalite layer at three different reduction times, from which it is evident that the matte phase in the fayalite layer decreases gradually with the increase in reduction time. There are two reasons for this behavior. First, with the increase in reduction time, the Fe_3O_4 content in the slag decreases and therefore the slag viscosity decreases, and this is beneficial for the settling of matte. Secondly, the settling time for the matte also increases with the increase in reduction time, which is conducive to the formation of the matte layer.

Based on EMPA analysis, it was found that a layer adheres to the matte layer of the three samples. In view of this phenomenon, the samples with reduction time of 30 minutes were selected for further examination. Figure 10 shows the microstructure of the interface between the fayalite layer and the matte layer of the sample in Figure 5(a). Table III shows the elemental composition of point 1 and point 2 in Figure 10(a) from which it is clear that point 1, corresponding to the interfacial layer, and point 2 consist of the phases

magnetite and fayalite, respectively. As mentioned previously, magnetite particles are adsorbed on the surface of matte droplets.^[10,13] These matte-magnetite particles deposit together to the bottom of the slag.^[10,14] At a later stage, the magnetite phase is gradually precipitated with the decrease in temperature and enriched in the upper part of the matte layer. The existence of the magnetite layer increases the viscosity of surface of matte layer and hinders the further settlement of matte.^[15]

Figure 11 shows the cross-sections and copper content of slag samples with reduction time of 30 minutes and reduction temperatures of 1250 °C, 1275 °C, 1300 °C, and 1325 °C, respectively. At 1250 °C, foaming slag is formed. With the increase of reduction temperature, the phenomenon of foaming slag gradually disappears indicating that temperature has a significant effect on foam formation. This is attributed to the improved fluidity of slag with increasing temperature, which is beneficial for the release of bubbles. It can be seen from Figure 11(e) that the copper content in slag decreases from 8.48 to 1.14 pct with the increase in reduction temperature. When the reduction temperature is low, the content of Fe_3O_4 in slag and the viscosity of the slag are high, magnetite and matte will form composite particles which are suspended in the slag and hinder the settlement of matte. With the increase in temperature, the viscosity of the slag decreases, and this is beneficial for the settlement of matte droplets.

B. Effect of Sulfur on Fe_3O_4 Content in Slag

The effect of sulfur on reduction rate is studied by adding cuprous sulfide (Cu_2S) to copper slag to change the content of sulfur in slag. Figure 12 shows the cross-sections of copper slag with different sulfur content, reduction temperature of 1250 °C and reduction time of 30 minutes. The sulfur contents of the samples in Figures 12(a), (b), (c) and (d) are 8.02, 8.5, 9, and 10 wt pct, respectively. Figure 13 shows the Fe_3O_4 content and copper content in the slag of the four samples in Figure 12. It can be seen from Figure 12 that with the increase of sulfur content in slag, the volume of matte at the bottom of slag decreases gradually. It can be seen from Figure 13 that the content of Fe_3O_4 and copper in

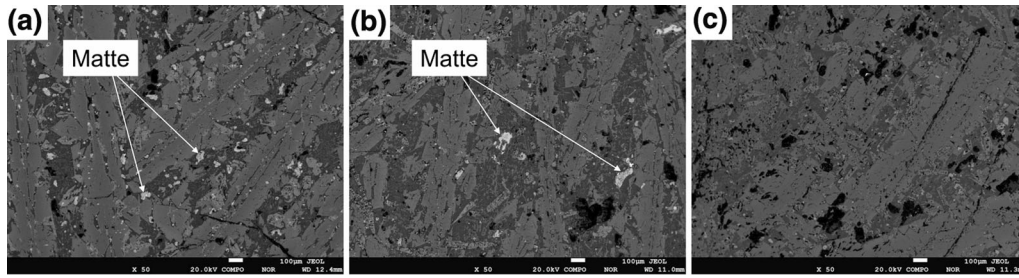


Fig. 9—Microstructure of fayalite layers with different reduction times at 1250 °C: (a) 30 min; (b) 60 min; (c) 90 min.

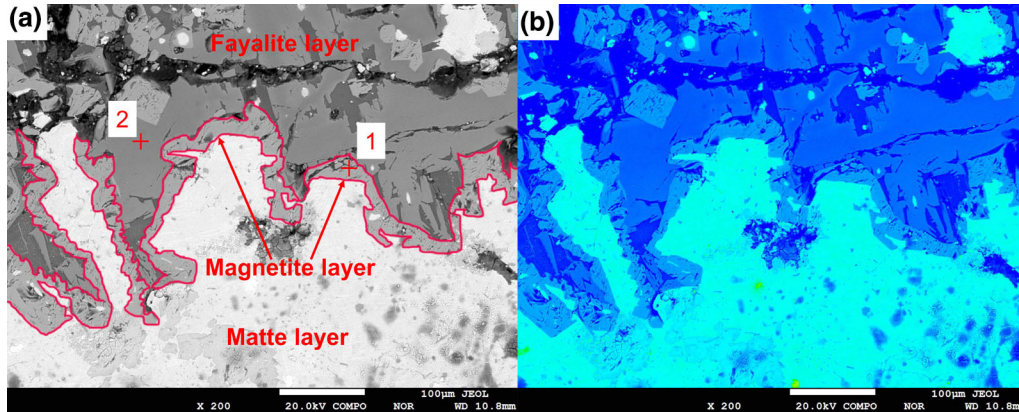


Fig. 10—Microstructure of the interface between the fayalite layer and the matte layer with reduction time of 30 min at 1250 °C: (a) original image; (b) color image (Color figure online).

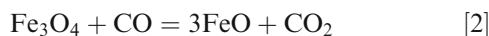
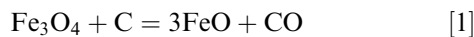
Table III. Elemental Analysis of Different Phases (Wt Pct)

Point	O	Si	S	Fe
1	24.84	0	0	71.63
2	33.30	15.09	0	44.52

slag increases with the increase of sulfur content in slag. According to the above experimental results, increasing the sulfur content in the slag is not conducive to the reduction reaction of Fe_3O_4 and graphite rod. The existence of unreduced Fe_3O_4 leads to the increase of slag viscosity, which is not conducive to the settlement of matte.

C. Kinetics of Fe_3O_4 Reduction

The reduction of Fe_3O_4 in molten slag is a multiphase process which can be represented as follows:



At the initial stage of the reaction, Fe_3O_4 in the slag and the graphite rod are in direct contact and Fe_3O_4 is reduced to FeO by C. However, as shown by reaction [1], the interface between slag and the graphite rod is then separated by a gas product. The gas film formed at the interface between slag and the graphite rod reduces the direct contact area between the liquid slag and graphite, and new reaction interfaces between gas-slag and gas-graphite are formed. A schematic representation of the reduction of Fe_3O_4 in slag by the graphite rod is shown in Figure 14.^[16]

The reduction reaction of graphite rod and Fe_3O_4 in molten slag consists of the following steps^[17,18]:

- (1) Produced CO diffusion into the slag layer.
- (2) Slag-gas interface reaction occurs, *i.e.*, Fe_3O_4 reacts with CO to form CO_2 .
- (3) Produced CO_2 diffuses to the gas-graphite interface.
- (4) Boudouard reaction occurs at the gas-graphite interface to produce CO gas.
- (5) Part of CO is separated from the reaction interface by growth and rupture and diffuses to the slag-gas interface.

Therefore, possible limiting steps for the reduction process are the following: ①Diffusion of CO and CO_2 within the slag. ②Indirect reduction of Fe_3O_4 at slag-gas interface. ③Boudouard reaction. In the following section, kinetic parameters are calculated to determine which of these processes is the limiting step for the reduction of Fe_3O_4 by the graphite rod.

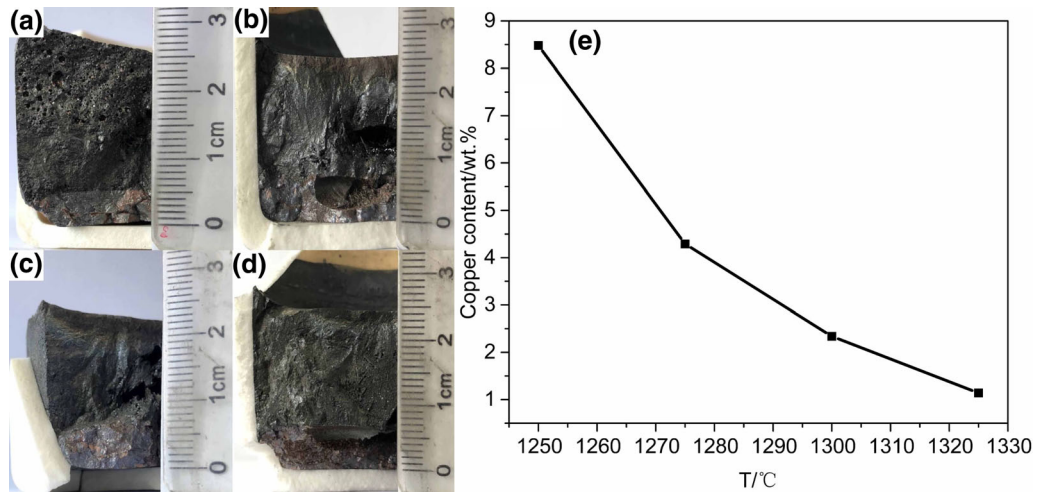


Fig. 11—Cross-sections and copper content of slag samples with reduction time of 30 min at different temperatures: (a) 1250 °C; (b) 1275 °C; (c) 1300 °C; (d) 1325 °C; (e) copper content of sample.

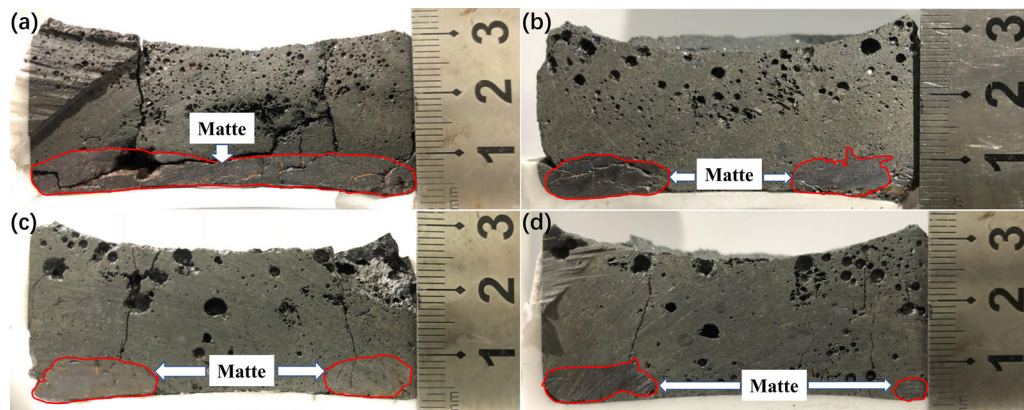


Fig. 12—Cross-sections of slag samples with different sulfur content: (a) 8.02 wt pct; (b) 8.5 wt pct; (c) 9 wt pct; (d) 10 wt pct.

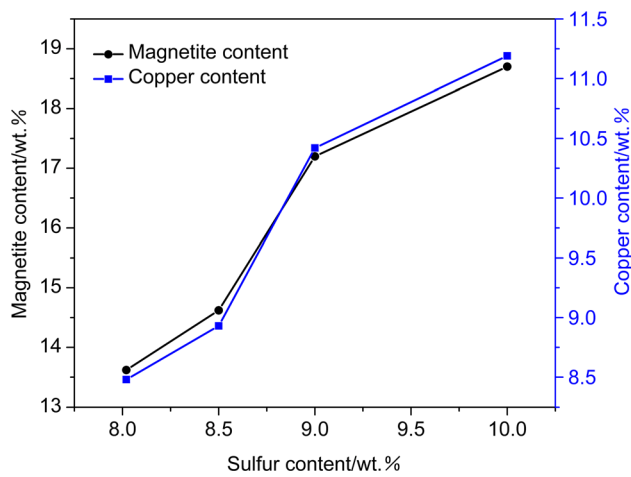


Fig. 13—Fe₃O₄ content and copper content of slag samples with different sulfur content.

D. Reaction order and apparent activation energy

The reaction rate relationships are shown in Table IV.^[19]

The rate of reduction of Fe₃O₄ in molten slag by the graphite rod can be expressed as Eq. [4].^[20,21]

$$v = -\frac{dw}{dt} = -w_s \frac{dC}{dt} = kAC^\alpha \quad [4]$$

where v is the reduction rate, g/min, w_s is the quantity of molten slag, g, C is the weight percent of Fe₃O₄ in slag, A is the interfacial area, cm², k is the apparent reaction rate constant, g/cm² min, and α is the reaction order.

In this study, the initial content of Fe₃O₄ in slag is less than 15 pct, oxygen atoms from Fe₃O₄ are consumed during the reduction process. Therefore, it is considered that the weight of slag remains essentially constant during the reduction process. The initial contact area between molten slag and the graphite rod was used as the interfacial area to calculate the reaction rate.^[22] The thickness of the static slag is 3 cm and the contact area between the graphite rod and the slag is 11.3 cm². Rearranging Eq. [4] gives Eq. [5]:

$$-\frac{dC}{dt} = \frac{kA}{w_s} C^\alpha \quad [5]$$

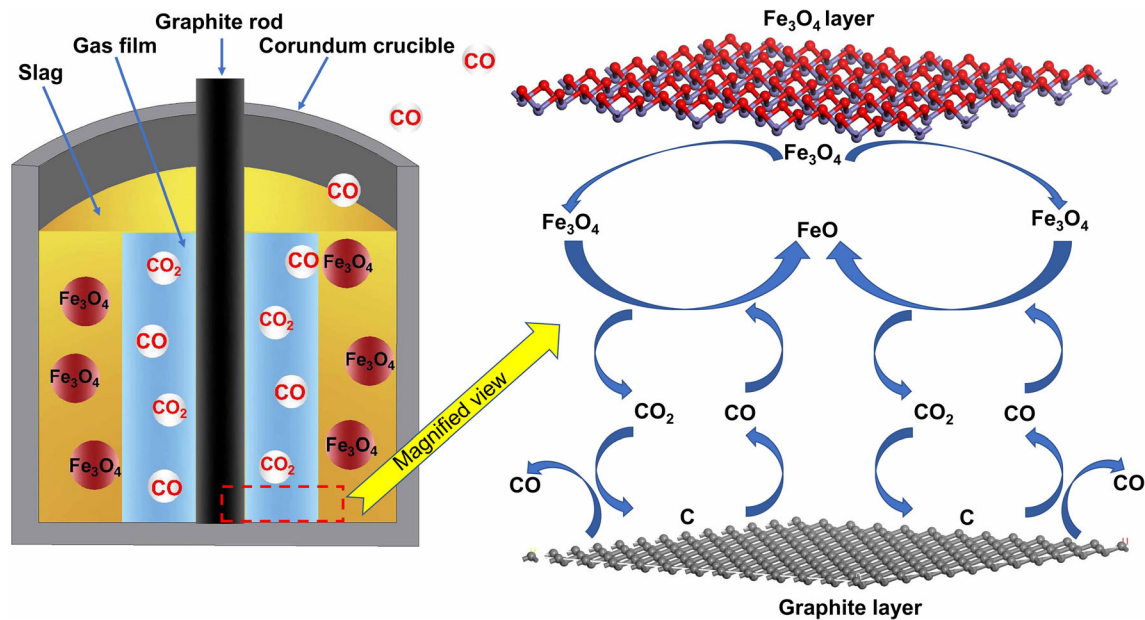


Fig. 14—Schematic representation of the reduction of Fe_3O_4 in molten slag by the graphite rod.

Table IV. Reaction Rate Relationships

Reaction Order	Reaction Rate Equation	Integral Equation of Reaction Rate
0	$-\frac{dC}{dt} = k$	$C_0 - C = kt$
1	$-\frac{dC}{dt} = kC$	$-\ln \frac{C}{C_0} = kt$
2	$-\frac{dC}{dt} = kC^2$	$\frac{1}{C} - \frac{1}{C_0} = kt$

The integral of Eq. [5] can be expressed as:

$$\alpha = 0, C_0 - C = \frac{kA}{W_S} t = F(C) \quad [6]$$

$$\alpha = 1, -\ln \frac{C}{C_0} = \frac{kA}{W_S} t = F(C) \quad [7]$$

$$\alpha = 2, \frac{1}{C} - \frac{1}{C_0} = \frac{kA}{W_S} t = F(C) \quad [8]$$

Equations [6], [7], and [8] represent the relationship between the concentration of Fe_3O_4 in slag and time for different reaction orders. C_0 is the initial weight percent of Fe_3O_4 in slag, and C is the weight percent of Fe_3O_4 in slag at different times.

Figure 15 shows the $F(C)$ - v - t relationships at different reduction temperatures (a: 1250 °C, b: 1275 °C, c: 1300 °C, d: 1325 °C). From the linear character of the curve, the reaction order can be determined and the apparent reaction rate constant k can be calculated. When the reaction order is 2, $F(C)$ - v - t has the strongest linear relationship. Therefore, the reduction of Fe_3O_4 is

in accord with a second-order reaction at the temperature range of 1250 °C to 1325 °C. Table V shows that the apparent reaction rate constant based on the slope of the $F(C)$ - v - t relationships increases with temperature. This is consistent with the fact that with increasing temperature, the slag viscosity decreases, the activity of Fe_3O_4 increases, both of which improve the diffusion and promote the reduction of Fe_3O_4 in the slag.

According to the Arrhenius equation (Eq. (9)), for the relationship between $\ln k$ and $1/T$, the apparent activation energy can be calculated from the slope of the curve.

$$\ln k = -\frac{E}{RT} + \ln A \quad [9]$$

where E is the apparent activation energy of the reaction, J/mol, A is the pre-exponential factor, R is 8.314 J·mol⁻¹·K⁻¹, and T is the system temperature, K.

Figure 16 shows the relationship between $\ln k$ and $1/T$ for a temperature range of 1250 °C to 1325 °C and provides an apparent activation energy value of 610 kJ/mol. When the apparent activation energy is greater than 400 kJ/mol, the reaction is generally controlled by interfacial chemical reaction.^[23,24] It can be concluded

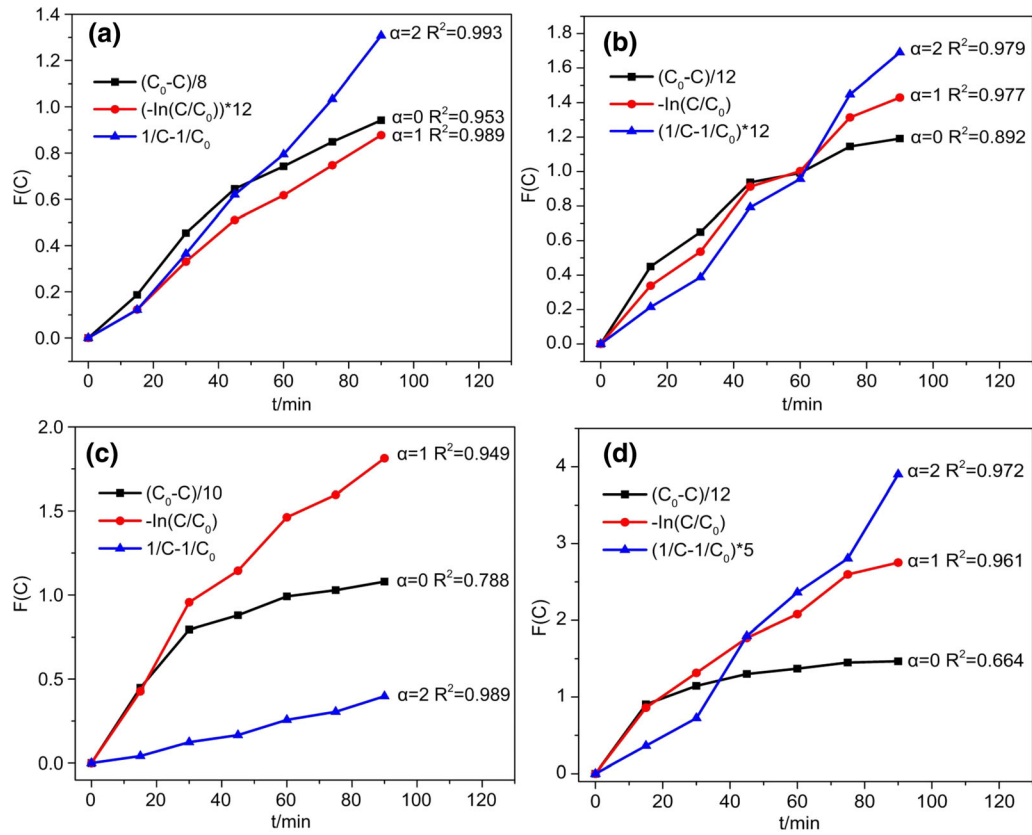


Fig. 15— $F(C)$ - v - t relationships for different reaction orders: (a) 1250 °C; (b) 1275 °C; (c) 1300 °C; (d) 1325 °C.

Table V. Apparent Reaction Rate Constants in the Temperature Range 1250 °C to 1325 °C

	1250 °C	1275 °C	1300 °C	1325 °C
k	0.0326	0.0754	0.1170	0.3487

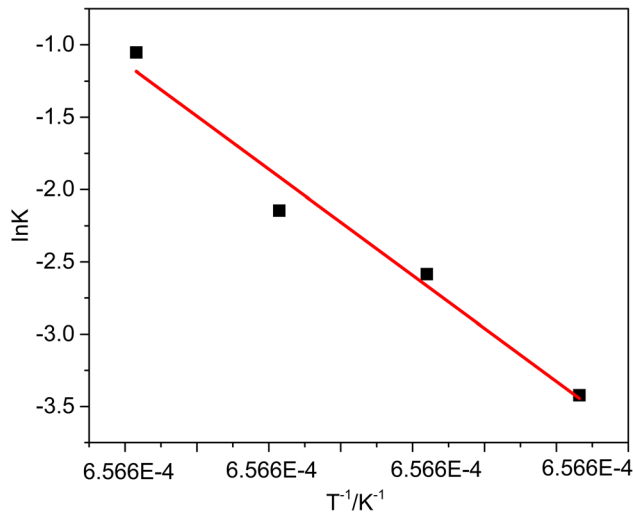


Fig. 16—Relationship between $\ln k$ and $1/T$ in the temperature range of 1250 °C–1325 °C.

therefore that the diffusion of CO and CO₂ is not limiting step and that the reduction of Fe₃O₄ in slag is controlled by the interface chemical reaction. According to Jung's research,^[25] in the process of reducing Fe₃O₄ to FeO by carbon, the consumption rate of CO is higher than the formation rate of CO from the Boudouard reaction. This shows that the reaction rate between Fe₃O₄ and CO is faster than the rate of the Boudouard reaction. Based on this analysis, the limiting step for the reduction reaction of Fe₃O₄ in slag by the graphite rod is the Boudouard reaction.

IV. CONCLUSIONS

In this study, a graphite rod was used to reduce Fe₃O₄ in copper smelting slag. The matte particles in the foaming slag are coated with fayalite and magnetite phases. With increase of reduction temperature and reduction time, slag foaming progressively disappears. The increase of sulfur content in slag will reduce the reaction rate of Fe₃O₄ and graphite rod, which is not conducive to the settlement of matte. The apparent reaction rate constant increases with increase in temperature, the apparent activation energy is 610 kJ/mol, and the limiting step is the Boudouard reaction.

ACKNOWLEDGMENTS

Financial support for this study was provided by the National Natural Science Foundation of China (Nos. U1602272, 51664039, and 51764035).

REFERENCES

1. Z.H. Yang, Q. Lin, S.C. Lu, Y. He, G.D. Liao, and Y. Ke: *Ceram. Int.*, 2014, vol. 40, pp. 7297–305.
2. J. Zhang, Y.H. Qi, D.L. Yan, X.L. Cheng, and P. He: *J. Iron. Steel Res. Int.*, 2015, vol. 2, pp. 121–27.
3. J. Zhang, Y.H. Qi, D.L. Yan H.C. Xu: *J. Iron Steel Res. Int.*, 2015, vol. 5, pp. 396–401.
4. L. Miganei, E. Gock, M. Achimovicová, L. Koch, H. Zobel, and J. Kähler: *J. Clean Prod.*, 2017, vol. 164, pp. 534–42.
5. Y. Shi, Y.G. Wei, S.W. Zhou, B. Li, Y.D. Yang, and H. Wang: *J. Alloys Compd.*, 2020, vol. 822, pp. 153478–84.
6. S.W. Zhou, Y.G. Wei, B. Li, and H. Wang: *Metall. Mater. Trans. B*, 2018, vol. 49B, pp. 3086–96.
7. R.G. Reddy, V.L. Prabhu, and D. Mantha: *High Temp. Mater. Process.*, 2003, vol. 22, pp. 25–33.
8. S. Jahanshahi and S. Wright: *Metall. Mater. Trans. B*, 2017, vol. 48B, pp. 2057–66.
9. B. Li, Y.G. Wei, H. Wang, and Y.D. Yang: *ISIJ Int.*, 2018, vol. 58, pp. 1168–74.
10. S.W. Zhou, Y.G. Wei, Y. Shi, B. Li, and H. Wang: *Metall. Mater. Trans. B*, 2018, vol. 49B, pp. 2458–68.
11. J. Martinsson, B. Glaser, and S. Du: *Metall. Mater. Trans. B*, 2016, vol. 47, pp. 1–4.
12. A. Davydenko, A. Karasev, G. Lindstrand, and P. Jonsson: *Steel Res. Int.*, 2015, vol. 86, pp. 146–53.
13. S.W. Li, J. Pan, D.Q. Zhu, Z.Q. Guo, J.W. Xu, and J.L. Chou: *Powder Technol.*, 2019, vol. 347, pp. 159–69.
14. E.D. Wilde, I. Bellemans, L. Zheng, M. Campforts, M. Guo, B. Blanpain, N. Moelans, and K. Verbeken: *Mater. Sci. Technol.*, 2016, vol. 32, pp. 1911–24.
15. G.R. Qu, Y.G. Wei, B. Li, H. Wang, Y.D. Yang, and A. McLean: *J. Alloys Compd.*, 2020, vol. 824, pp. 15910–18.
16. C.B. Wu, J.B. Zhang, Q.J. Wu, and L. Yue: *J. Chongqing Univ.*, 2015, vol. 38, pp. 11–16.
17. S.N. Lekakh and B. Hrebec: *Int. J. Metalcast.*, 2016, vol. 10, pp. 1–12.
18. D.Y. Kim, I.H. Jeong, and S.M. Jung: *Ironmak. Steelmak.*, 2015, vol. 43, pp. 526–32.
19. X.L. Huang: *Iron and Steel Metallurgy (Ironmaking Part)*, Metallurgical Industry Press, Beijing, 2000, pp. 413–38.
20. Y.G. Guo, R. Zhu, Z.Z. Fei, M.S. Ma, Y. Wang, and J. Liu: *China Nonferrous Metall.*, 2017, vol. 5, pp. 75–80.
21. G. Wang, Q.G. Xue, Y.F. Shen, and J.S. Wang: *Chin. J. Eng.*, 2016, vol. 5, pp. 623–29.
22. Z.Z. Huang, X.G. Xiao, and Z.Q. Xiao: *Chin. J. Process Eng.*, 1994, vol. 4, pp. 283–88.
23. H.M. Long, J.X. Li, P. Wang, and S.Q. Shi: *Ironmak. Steelmak.*, 2012, vol. 39, pp. 585–92.
24. J.L. Zhang, Z.Y. Wang, X.D. Xing, Z.J. Liu, and X.L. Liu: *J. Cent. South Univ. (Sci. Technol.)*, 2015, vol. 46, pp. 41–48.
25. S.M. Jung and S.H. Yi: *Ironmak. Steelmak.*, 2014, vol. 41, pp. 38–46.

Publisher's Note Springer Nature remains neutral with regard to jurisdictional claims in published maps and institutional affiliations.